STRUCTURAL BIOLOGY

# Optimal anchoring of a foldamer inhibitor of ASF1 histone chaperone through backbone plasticity

**Johanne Mbianda[1]*†, May Bakail[2,3]*‡, Christophe André[1], Gwenaëlle Moal[2,3], Marie E. Perrin[2,3], Guillaume Pinna[2,3], Raphaël Guerois[2,3], Francois Becher[2], Pierre Legrand[4], Seydou Traoré[2,3], Céline Douat[1]§, Gilles Guichard[1]||, Françoise Ochsenbein[2,3]||**



**Sequence-specific oligomers with predictable folding patterns, i.e., foldamers, provide new opportunities to mimic α-helical peptides and design inhibitors of protein-protein interactions. One major hurdle of this strategy is to retain the correct orientation of key side chains involved in protein surface recognition. Here, we show that the structural plasticity of a foldamer backbone may notably contribute to the required spatial adjustment for optimal interaction with the protein surface. By using oligoureas as α helix mimics, we designed a foldamer/peptide hybrid inhibitor of histone chaperone ASF1, a key regulator of chromatin dynamics. The crystal structure of its complex with ASF1 reveals a notable plasticity of the urea backbone, which adapts to the ASF1 surface to maintain the same binding interface. One additional benefit of generating ASF1 ligands with nonpeptide oligourea segments is the resistance to proteolysis in human plasma, which was highly improved compared to the cognate α-helical peptide.**

## INTRODUCTION

The synthesis of sequence-specific synthetic oligomers that fold into well-defined helical structures has opened up enticing opportunities for mimicking α-helical peptides and addressing some of their limitations in biomedical applications (*1*–*5*). The improved resistance to proteolysis demonstrated by a number of peptidomimetic foldamer backbones including peptoids (*6*), β- and γ-peptides (*7*–*9*), γ-AA-peptides (*10*), N,N′-linked oligourea foldamers (*11*), and many others (*1*–*4*) is a significant advantage that can translate into increased duration of action. Moreover, the use of artificial backbones as α helix mimics can lead to ligands with unusual receptor-activation profiles (*12*, *13*), inhibitors of protein-protein interactions with increased selectivity (*14*) and cell permeability (*10*, *15*). However, one challenge associated with the use of foldamers for specific recognition of protein surface is to position the side chains at the surface of the foldamer with the correct spacing and orientation to maintain key contacts with the targeted protein surface. One emerging approach to elaborate such ligands consists in redesigning α-helical peptides by combining α-peptide and foldamer backbones in a single chain. This has been successfully achieved with α/β-peptides by introducing regularly spaced β-amino acid residues to replace α-amino acids along the sequence of interest (*16*–*18*). Similarly, we have recently shown that peptide-oligourea replacements can be used to produce analogs of class B G protein–coupled receptor (GPCR) ligands with improved duration of action and to mimic protein tertiary folds (*19*, *20*). The choice of replacing a peptide segment with an oligourea insert is explained by the similarity and compatibility of the two helical folds and by the possibility to control the nature and the distribution of side chains at the surface of the oligourea helix (*21*). In the work on GPCR ligands (incretins), we actually scanned the entire helical portion of the peptide by swapping four consecutive amino acids for three ureido residues ($Ala^{u}Ala^{u}Ala^{u}$ scan) to identify the most effective positions for oligourea inserts (*19*). However, the impact of replacing key anchor residues at sites that directly contact a protein surface by an oligourea foldamer has not yet been examined in detail. This is particularly relevant if one aims to develop short oligourea/peptide hybrids that can disrupt protein-protein interactions. To address this question and investigate how to appropriately position side chains along the oligourea backbone while retaining recognition properties, we selected antisilencing function 1 (ASF1) histone chaperone as a protein target.

Histone chaperones regulate histone dynamics within chromatin and the establishment of numerous epigenetic markers (Fig. 1A). Their dysfunction is associated with a number of pathologies including aging-related diseases, pathogen infections, or cancer (*22*). ASF1 histone H3-H4 chaperone is critically involved in nucleosome assembly/disassembly and regulation of gene expression. In human, two ASF1 paralogs exist, called ASF1A and ASF1B. They share 70% of sequence identity and exhibit redundant and specific functions (*23*). Depletion of ASF1A/ASF1B or ASF1A + ASF1B has been shown to block proliferation in various cancer cell lines and to sensitize cells to chemotherapeutic agents such as doxorubicin (*24*). Overexpression of ASF1B in patients with breast cancer is a marker of poor prognosis (*25*), while ASF1A overexpression is observed in liver, prostate, or gastric carcinoma (*26*, *27*). Together, these findings make ASF1A/ASF1B appealing biological targets for innovative anticancer treatments.

Details of the interaction between ASF1 and its protein partners including H3-H4 have been gathered at atomic resolution and involve a binding surface fully identical for both paralogs (Fig. 1B)

[1]Univ. Bordeaux, CNRS, Bordeaux INP, CBMN, UMR 5248, Institut Européen de Chimie et Biologie, 2 rue Robert Escarpit, F-33607 Pessac, France. [2]Institute Joliot, Commissariat à l'énergie Atomique (CEA), Direction de la Recherche Fondamentale (DRF), CEA Saclay, F91191 Gif-sur-Yvette, France. [3]Institute for Integrative Biology of the Cell (I2BC), CEA, CNRS, Université Paris-Saclay, 91198, Gif-sur-Yvette cedex, France. [4]Synchrotron SOLEIL, L'Orme des Merisiers, F91190 Gif-sur-Yvette, France.
*These authors contributed equally to this work.
†Present address: School of Chemistry, University of Southampton, Southampton SO17 1BJ, UK.
‡Present address: Institute of Science and Technology Austria Campus IT Am Campus 1, 3400 Klosterneuburg, Austria.
§Present address: Department of Pharmacy and Center for Integrated Protein Science, Ludwig-Maximillians-Universität, Butenandtstr. 5-13, 81377 München, Germany.
||Corresponding author. Email: g.guichard@iecb.u-bordeaux.fr (G.G.); francoise.ochsenbein@cea.fr (F.O.)

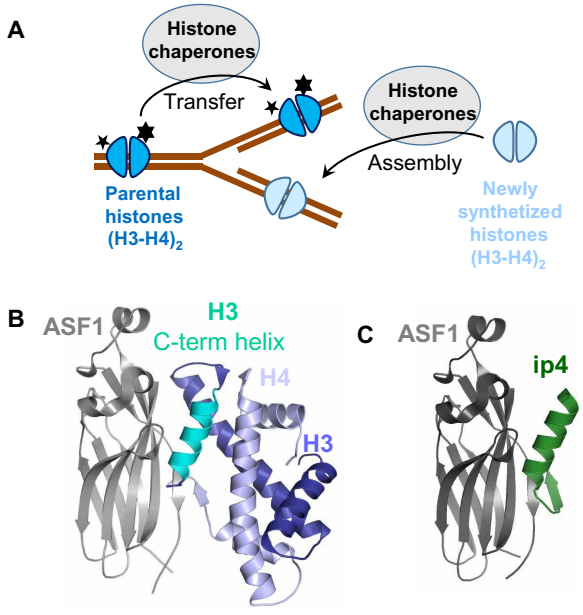


**Fig. 1. The histone chaperone ASF1 target.** (**A**) ASF1 belongs to the histone chaperone family whose members are involved in the transfer and assembly of parental histones (which are highly modified and carry essential epigenetic marks represented as stars) and newly synthetized histones during the process of DNA replication. (**B**) Structure of the ternary complex hASF1A(1-175)-H3-H4 (pdb 2io5). (**C**) Structure of the complex hASF1A(1-156)-**ip4** (pdb 6foh) (*30*).

(*28*, *29*). The specific recognition of the heterodimeric H3-H4 complex by ASF1 involves several shallow pockets distributed over a large surface area that renders the use of small-molecule–based approaches highly challenging.

By using an iterative structure-guided approach, we recently designed a 26-residue peptide called **ip4**, ASTEEKWARLARRIAG-AGGVTLDGFG exhibiting an affinity for ASF1 in the low nanomolar range. This peptide is composed of two parts, an α-helical segment derived from histone H3 C terminal helix covalently linked to a β strand originating from histone H4 C terminus. The high-resolution structure of **ip4** in complex with ASF1 showed that its helical moiety interacts in a manner similar to histone H3 and harbors four of the five hot spot residues of the interaction ($Lys^2$, $Leu^6$, $Arg^9$, and $Ile^{10}$) (Fig. 1C and fig. S1) (*30*). Upon conjugation to a cell-penetrating peptide, **ip4** was able to translocate into cells, impair cell proliferation, and perturb the cell cycle progression similarly to the silencing of ASF1 (*30*). Injection of this conjugate in mouse allografts reduced tumor growth. However, further exploration of its therapeutic potential was early compromised by its sensitivity to protease degradation.

To address this limitation, we developed a strategy based on rational design and foldamer chemistry to mimic the α-helical part of **ip4** and reproduce its binding mode. Here, we report the identification of peptide-oligourea hybrids that recognize and bind to the surface of ASF1 as well as the first x-ray structure at atomic resolution of a foldamer ligand bound to this histone chaperone.

## RESULTS

### Defining the minimal helical part required for ASF1 binding

At first, we synthesized the hexadecapeptide **P1** corresponding to the α-helical segment of **ip4** as a reference of binding to ASF1. It

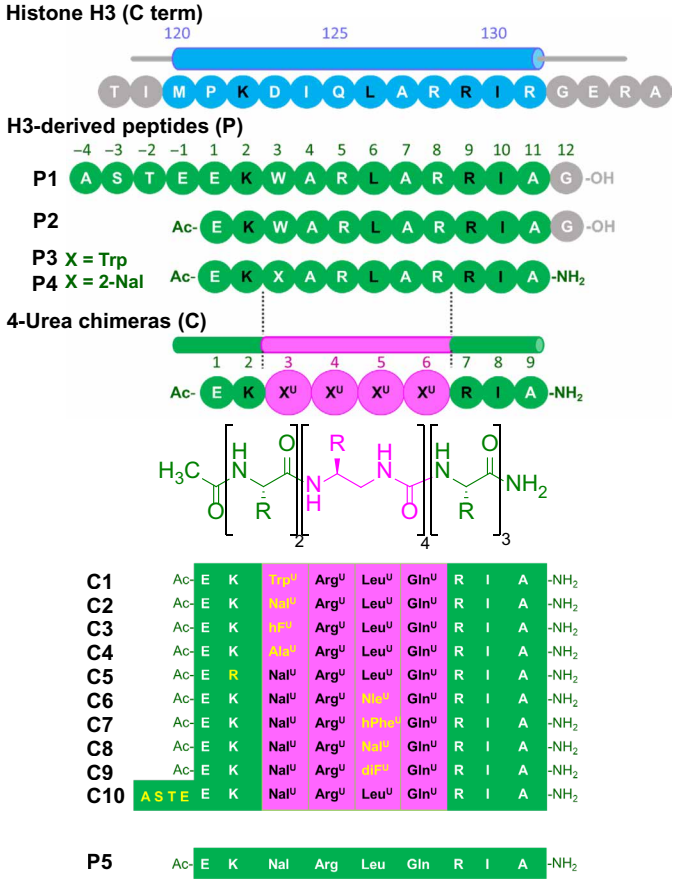


**Fig. 2. List of peptides (P) and 4-urea chimeras (C) synthetized and analyzed in this study.**

contains the four anchor residues, $Lys^2$, $Leu^6$, $Arg^9$, and $Ile^{10}$, that are buried in specific pockets upon binding and mainly interact with $Asp^{54}$, $Asp^{88}$, $Val^{94}$, $Leu^{96}$, $Tyr^{112}$, and $Arg^{146}$ residues at the surface of ASF1 (Fig. 2 and fig. S1). **P1** displays an affinity for the conserved domain of human ASF1A [hASF1A(1-156)] of 0.13 ± 0.04 μM as measured by isothermal titration calorimetry (ITC) (Table 1 and fig. S2), which is a 10-fold decrease in affinity with respect to **ip4**. This peptide has an N-terminal capping motif (Ala-Ser-Thr-Glu) and a C-terminal Gly residue, also known to favor helix capping (*31*). Because our goal was to prepare minimal foldamer sequences, we next synthesized two derivatives of **P1** missing the N-terminal capping motif and bearing either the C-terminal Gly residue (**P2**) or not (**P3**) (Fig. 2). These two peptides exhibited an affinity for hASF1A in the submicromolar range with $K_d$ = 0.44 ± 0.02 μM and 0.27 ± 0.07 μM for **P2** and **P3**, respectively (Table 1 and fig. S2). **P3** lacking both capping motifs showed a slight increase in affinity for ASF1 compared to **P2**. We thus decided to focus our design on sequences lacking the terminal Gly residue. As in **ip4**, peptides **P1** to **P3** contain a Trp in position 3 whose indole side chain enables favorable interactions with the apolar patch in ASF1 formed by $Val^{92}$ and $Tyr^{112}$. In our previous study, we showed that $Trp^3$ combined with the N-terminal capping motif led to a 10-fold increase in the affinity for ASF1 (*30*). With the aim to further improve apolar contacts with the surface of ASF1, we substituted $Trp^3$ in **P3** by a napthylalanine ($Nal^3$ in **P4**) (Fig. 2). The binding affinity remained in the

**Table 1. Binding affinities and thermodynamic parameters of peptides/chimeras for hASF1A determined by ITC measurements and NMR spectroscopy.**

| Peptide/chimera | $K_d$ (μM) *,† (ITC) | *N** | Δ*H** (kcal/mol) | −TΔS* (kCal/mol) | $K_d$ (μM)‡ (NMR) |
|---|---|---|---|---|---|
| **P1** | 0.13 ± 0.04 | 1.0 ± 0.1 | −11.7 ± 0.4 | 2.9 ± 0.4 | ND |
| **P2** | 0.44 ± 0.02 | 1.1 ± 0.2 | −10.3 ± 0.6 | 2.2 ± 0.6 | ND |
| **P3** | 0.27 ± 0.07 | 1.0 ± 0.1 | −10.5 ± 0.8 | 2.2 ± 0.9 | ND |
| **P4** | 0.20 ± 0.09 | 1.0 ± 0.1 | −9.2 ± 0.4 | 0.7 ± 0.6 | ND |
| **C1** | 10.6 ± 3.8 | 1.2 ± 0.2 | −3.6 ± 0.5 | −2.7 ± 0.7 | 18 ± 6 |
| **C2** | 2.7 ± 0.6 | 1.0 ± 0.1 | −2.2 ± 0.1 | −4.8 ± 0.2 | 4 ± 1 |
| **C3** | 4.6 ± 0.3 | 1.0 ± 0.1 | −3.3 ± 0.1 | −3.5 ± 0.7 | 6 ± 3 |
| **C4** | 13.3 ± 3.5 | 1.1 ± 0.2 | −1.8 ± 0.4 | −4.7 ± 0.5 | 15 ± 7 |
| **C5** | 6.6 ± 4.5 | 1.1 ± 0.1 | −3.5 ± 1.4 | −3.1 ± 0.2 | ND |
| **C6** | 4.3 ± 1.4 | 1.2 ± 0.1 | −2.2 ± 0.3 | −4.6 ± 0.4 | 8 ± 3 |
| **C7** | 15.4 ± 4.0 | 1.4 ± 0.2 | −1.7 ± 0.2 | −4.4 ± 0.4 | 16 ± 6 |
| **C8** | ND | ND | ND | ND | 152 ± 90 |
| **C9** | 7.9 ± 0.3 | 1.2 ± 0.3 | −3.5 ± 0.6 | −3.0 ± 0.5 | 7 ± 4 |
| **C10** | 13.1 ± 4.1 | 1.2 ± 0.2 | −1.9 ± 0.4 | −4.3 ± 0.2 | 18 ± 4 |

*ND, not determined. †Binding curves are shown in fig. S2. ‡Binding curves are shown in fig. S5.

same range as that of **P3**, but the analysis of the thermodynamic parameters indicated a more favorable contribution to binding entropy (Table 1 and fig. S2).

### Design of a peptide-oligourea chimera, mimicking the helical part of ip4

In a second round of design, we overlaid the x-ray crystal structure (pdb 6foh, Fig. 1C) of the Asf1-bound helical domain of **ip4** (i.e., sequence **P1**) with representative oligourea x-ray crystal structures to identify the optimal location for oligourea segment insertion (*21*, *32*). We decided to replace the six central α-residues in the sequence of **P3** and **P4** by four consecutive urea-type residues ($Xaa^U$ in Fig. 2). Models of the resulting 4-urea chimeras **C1** and **C2** were constructed assuming that the peptide-urea-peptide helices are fully formed. **C1** and **C2** distinguish from one another solely by a $Trp^U$ or a $Nal^U$ residue at position 3, respectively. Both chimeras were properly docked to ASF1 surface without generating major clashes (fig. S1, middle). In this model, it was indeed possible to place three of the four anchor residues very close to their respective position in the **ip4**/ASF1 x-ray crystal structure (α carbons of $Leu^{U5}$, $Arg^7$, and $Ile^8$, in **C2** matching those of $Leu^6$, $Arg^9$, and $Ile^{10}$ in **P1** by less than 1.5 Å, respectively). However, the fourth anchor, $Lys^2$, could not be properly aligned and lied away from the surface of ASF1, at more than 3 Å from its position in the **ip4**/ASF1 x-ray crystal structure (fig. S1, middle).

The **C1** and **C2** chimeras were prepared by solid phase synthesis using microwave assistance and appropriately protected succinimidyl carbamate building blocks for the construction of the oligourea segment (see the Supplementary Materials for details, table S1, and fig. S3) (*33*). The binding affinities of **C1** and **C2** for ASF1 were first measured by ITC (Table 1 and fig. S2). **C2** exhibits a low micromolar affinity for the protein target ($K_d$= 2.7 ± 0.6 μM), while **C1** has a fourfold weaker affinity, showing the beneficial effect of $Nal^{U3}$ residue over $Trp^{U3}$. Overall, **C1** and **C2** chimeras exhibit affinities 10 to 80 times lower than the **P1** to **P4** peptide series, with a 13-fold affinity drop of **C1** for ASF1 with respect to **P4**. In addition to binding affinities, microcalorimetry allowed us to measure the enthalpic and entropic contributions to the binding free energy for all peptides and chimeras (Table 1). Binding of **P1** to **P4** peptides to ASF1 is dominated by both a significant enthalpic contribution (Δ*H* ranging from −9.2 to −11.7 kcal/mol) and entropic cost (−TΔS ranging from 0.7 to 2.9 kcal/mol). In contrast, the enthalpic contribution of ASF1 binding to chimeras **C1** and **C2** (and also of all other chimeras analyzed in this study **C1** to **C10**) is much lower (Δ*H* ranging from −3.6 to −1.7 kcal/mol) but is associated with a favorable entropic contribution (−TΔS varying from −4.8 to −2.7 kcal/mol). This entropy-driven binding mode of chimeras could likely reflect their favorable structural preorganization with modest conformational entropy cost upon binding and/or favorable contribution of hydrophobic effect to the binding free energy. The modest enthalpy gain of chimeras upon ASF1 binding may account for a less optimized interface in terms of packing, H-bond network and/or electrostatics.

### NMR studies of chimera binding to ASF1

We next characterized the binding mode of **C1** and **C2** with ASF1 by nuclear magnetic resonance (NMR) spectroscopy and used **P1** binding as a reference. Increasing amounts of **C1** (or **C2**) were added to the N-terminal conserved domain of uniformly $^{15}$N-labeled hASF1A(1-156) (hereafter referred as $^{15}$N-hASF1A and see the Supplementary Materials for $^{15}$N-labeled protein production). Results are depicted in Fig. 3 and fig. S4. The maximal chemical shift variations (Δδ) were measured for most ASF1 residues at saturation concentration of chimeras or **P1** (fig. S4) and mapped on ASF1 surface (Fig. 3C, right). The binding site on ASF1 of both **C1** and **C2** hybrid foldamers was found to match that of histone H3 helical domain,

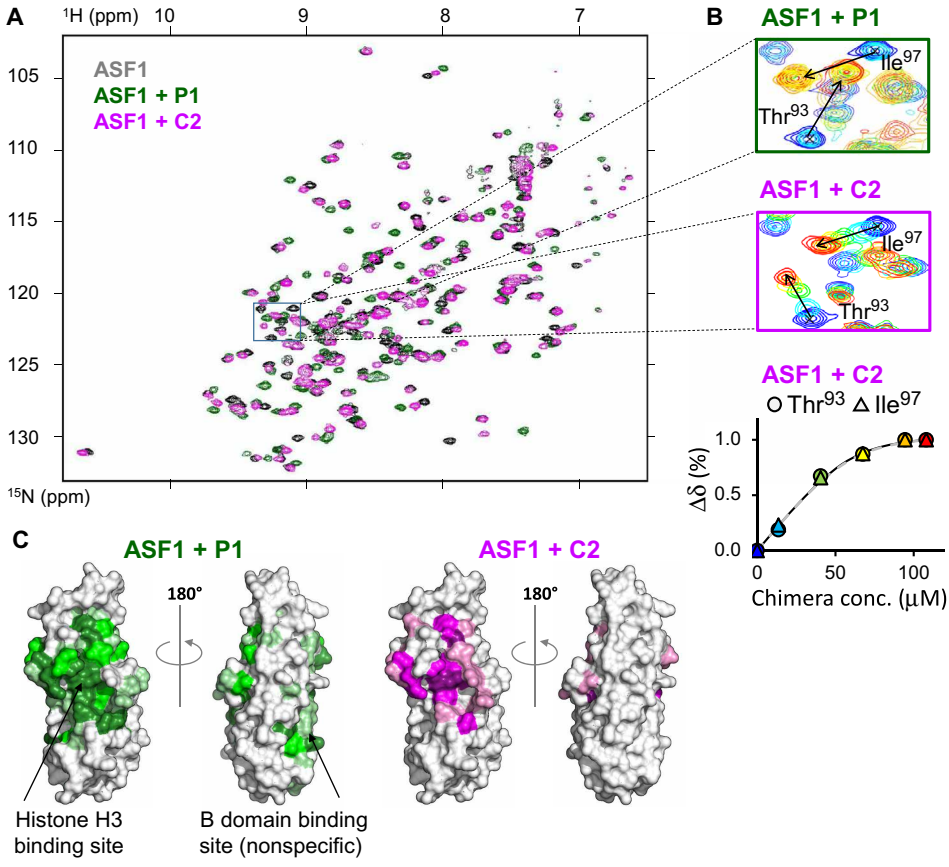


**Fig. 3. NMR analysis of P1 and C2 binding to ASF1.** (**A**) Overlay of the SOFAST HMQC spectra of $^{15}$N-hASF1A alone and after addition of a twofold excess of **P1** or **C2** (in gray, green, and magenta, respectively). The region indicated with a black box is magnified in (B, left and middle). (**B**) Top and middle: Overlay of five spectra measured at different concentrations of **P1** and **C2**, respectively, with a rainbow color code from blue to red (in dark blue, free hASF1A, and in red, after addition of twofold excess of peptide/chimera), for the region boxed in (A) showing the modification signals of Thr$^{93}$ and Ile$^{97}$ upon titration. The position of the signal in the bound state is indicated by an arrow. Bottom: Representative titration curve for ASF1 residues Thr$^{93}$ and Ile$^{97}$ using the same color code. The fitted curve is depicted as a dashed line. (**C**) Chemical shift mapping on hASF1A surface after addition of a twofold excess of **P1** or **C2** as indicated. Increasing color scale corresponds to higher chemical shift variations as in fig. S4.

also highlighted upon addition of **P1** (Fig. 3C, left, and fig. S4). Nonetheless, addition of **P1** also led to chemical shift perturbations for some ASF1 residues from Val$^{60}$ to Phe$^{72}$, matching the B-domain binding site (*34*). This corresponds to a nonspecific binding site for **P1**. **C1** and **C2** only interacted with the histone H3 binding site and did not give rise to such nonspecific binding (Fig. 3C, right, and fig. S4).

Upon $^{15}$N-ASF1 titration with **C2** as ligand (and also with all other chimeras **C1** to **C10** analyzed in this study), we observed a fast exchange rate, as illustrated by the recorded chemical shift variation (Δδ) of some hASF1A residues [Δδ of Thr$^{93}$ and Ile$^{97}$ displayed in Fig. 3B (middle)]. In contrast, **P1** to **P4** peptides showed a slow exchange regime upon interaction with ASF1 surface (Fig. 3B, top for **P1** titration). Although it is not possible to quantify the kinetic parameters from these NMR experiments, the fast exchange regime could reflect faster association/dissociation rates of the ASF1-chimera complexes compared to the ASF1-peptide ones. This hypothesis is compatible with a less optimized interface of the chimeras with respect to the peptides and consistent with the ITC results discussed above.

The fast exchange regime observed during the NMR titration experiments with the chimeras **C1** and **C2** allowed us to plot titration curves for several ASF1 residues interacting with each chimera [see the Materials and Methods section, Fig. 3B (right), and fig. S5]. The fitted affinity values are in good agreement with those measured by ITC (Table 1, last column).

As additional proof of the relevancy of our foldamer design, we synthesized the α-peptide **P5** having the exact side-chain composition of **C2** (Fig. 2). No binding to ASF1 was detected with this peptide by ITC (fig. S2). The chemical shift mapping presented in fig. S4 shows that upon titration of ASF1 with **P5** as ligand, we only observed small shifts of ASF1 residues in the B-domain nonspecific binding region. These results confirm that the binding of **C2** in the H3 binding pocket of ASF1 corresponds to specific interactions.

## High-resolution structure of C2 bound to ASF1

With the aim of gaining additional structural information about the binding mode of the peptide-oligourea hybrids to ASF1, we solved the cocrystal structure of **C2** bound to hASF1A conserved domain at 1.8-Å resolution. The structure confirms that overall **C2** binds ASF1 with the expected geometry [Fig. 4, figs. S1 (right) and S6A, and table S2]. The four anchoring side chains are positioned in a similar way to their cognate residues in hASF1A-bound **ip4** (fig. S6B).

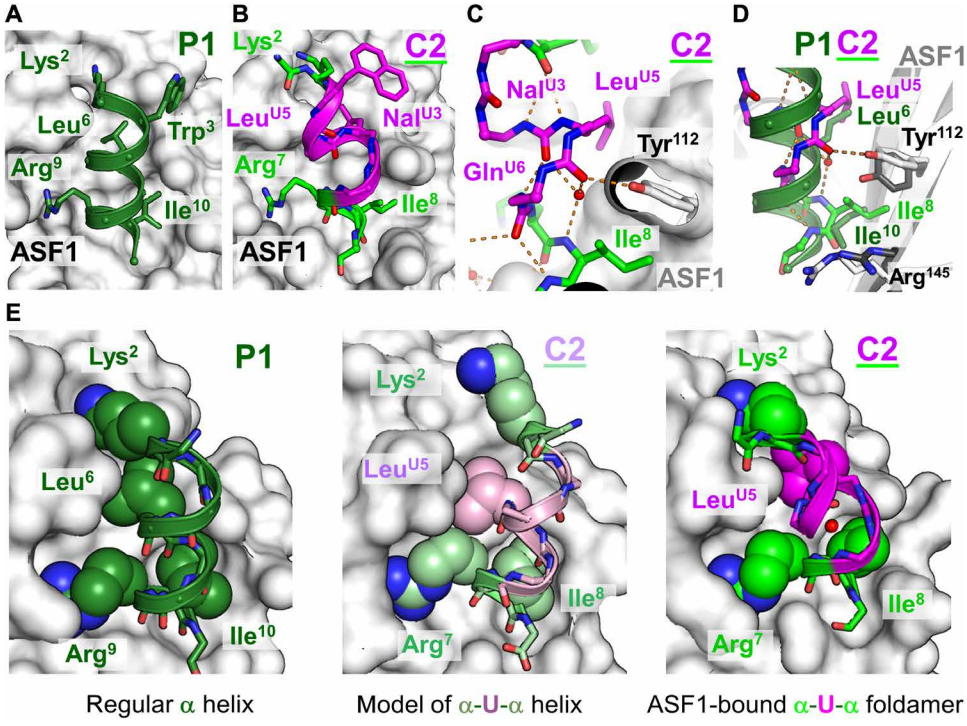


**Fig. 4. Crystal structure of chimera C2 in complex with ASF1 compared to the binding mode of P1.** (**A**) Front view of ASF1 (gray surface) bound to the peptide **P1** (green cartoon representation). Selected side chains of **P1** residues contacting ASF1 surface are highlighted. (**B**) Crystal structure of **C2** (sticks representation) bound to ASF1 (gray surface). **C2** α-amino acids are colored in green, and the four ureido-residue groups are in pink. (**C**) Detailed view of the conformation of **C2** in its central region with the same color code as in (B). Hydrogen bonds are shown with orange dashed lines; selected water molecules are shown with red spheres. (**D**) Overlay of **P1** and **C2** bound to ASF1. **C2** and **P1** backbones are shown with sticks or cartoon, respectively. For the sake of clarity, only the side chain of the two ASF1 residues with the greatest structural variations between the two structures is shown (in light gray for **C2**-bound ASF1 and in black for P1-bound ASF1). Most side chains of the chimera/peptide are also omitted; only $Leu^{U5}$/$Leu^{6}$ and $Leu^{8}$/$Leu^{10}$ of **C2** and **P1**, respectively, are shown in sticks and labeled. (**E**) ASF1 bound to **P1**, modeled **C2**, and **C2** in the crystal structure are depicted on the left, middle, and right, respectively. ASF1 is displayed as a gray surface; peptides and chimera backbones are displayed as sticks with hydrogen bonds as orange dashed lines. The four anchor residue side chains are shown as spheres and labeled. The water molecule bridging $Leu^{U5}$ carbonyl and $Ile^{8}$ amide bond is also shown as a red sphere.

This finding was unexpected, since in the original design with a canonical straight hybrid helix, $Lys^{2}$ side chain was not oriented toward its anchoring position (Fig. 4E, middle). As regard the peptide/urea chimera backbone, it adopts a helical conformation. Yet, the urea helix is unexpectedly distorted with respect to a regular 2.5 helix uniquely composed of urea-type units (Fig. 4, C and E, right) (*35*). The backbone hydrogen bond network is disrupted between $Nal^{U3}$ carbonyl and the amides of the urea bond $Leu^{U5}$-$Gln^{U6}$, and a water molecule bridges $Leu^{U5}$ carbonyl and $Ile^{8}$ amide bond (Fig. 4C). It is unlikely that this distortion is an intrinsic consequence of the hybrid character of the oligomer sequence as previous structural investigations of model peptide-oligourea hybrids showed formation of homogeneous helices without disruption of the H-bond network between the two segments (*21*). Alternatively, a mutual conformational adaptation between the protein and **C2**, together with the establishment of new specific contacts between the foldamer backbone and the protein, may account for this distortion. Several observations support this interpretation. First, a direct H-bond between the phenol group of $Tyr^{112}$ and the main chain urea carbonyl of residue $Leu^{U5}$ is formed (Fig. 4, C and D), and the intramolecular H-bond network of the chimeric helix is locally interrupted at this residue. This distortion can be further stabilized by the insertion of the $Leu^{U5}$-$Ile^{8}$ water bridge (Fig. 4, C and D). Overall, the orientation of several ASF1 side chains (such as $Tyr^{112}$ and $Arg^{145}$) is modified upon **C2** binding when compared to the **ip4** binding (Fig. 4D). This side-chain conformational rearrangement is possibly taking place for shaping the surface to the slight modifications in $Leu^{U5}$ and $Ile^{8}$ geometry. Last, the helix distortion induces a bending favorable for the anchor residue $Lys^{2}$ to interact with the acid loop of ASF1. Moreover, the tilted conformation of the hybrid helix facilitates the interaction of $Lys^{2}$ with $Asp^{88}$ as for **ip4** bound to ASF1 (Fig. 4E and fig. S6B). Together, these observations highlight the remarkable plasticity of the urea chimeric helix, able to kink to adapt ASF1 surface and optimize interactions with the four anchoring residues.

A second noticeable feature of bound **C2** in the crystal structure is that the $Nal^{U3}$ residue does not interact with the expected ASF1 residues ($Tyr^{112}$ and $Val^{92}$). In contrast, the $Nal^{U3}$ side chain associates with a symmetrical ASF1 molecule in a pocket containing the $Val^{60}$-$Phe^{72}$ stretch corresponding to the B-domain binding region of ASF1 (fig. S6C). This interaction is most probably a crystallization artifact since this binding site was not highlighted in the NMR chemical shift mapping in solution upon addition of **C2** to $^{15}$N-hASF1 as mentioned in the previous section (Fig. 3C and fig. S4). To further validate this hypothesis, we synthetized two additional variants of **C2** equipped either with a smaller ($hPhe^{U3}$ in **C3**) or no aromatic ring ($Ala^{U3}$ in **C4**) (Fig. 2). We next measured their

respective affinity for ASF1 by ITC and NMR (Table 1 and fig. S2). A slight decrease in affinity (twofold) was observed for **C3**, whereas a more pronounced effect on binding was measured with **C4**. These data support the conclusion that the naphtyl ring of $Nal^{U3}$ participates in the interaction, despite the absence of direct contact in the x-ray crystal structure of the ASF1/**C2** complex. We thus conclude that the chimera **C2** at the $Nal^{U3}$ residue could adopt a different rotamer in solution than the one selected in the crystal, but this conformation might be rather dynamic due to sparse packing. Together, structural data reported here validate the mode of interaction of **C2** with ASF1 as well as our general design approach.

We next attempted to modulate the recognition of ASF1 by hybrid foldamers through sequence manipulations. As already discussed in the x-ray crystal structure of ASF1/**C2** complex, $Lys^2$ is properly oriented and establishes electrostatic interactions with ASF1-$Asp^{88}$ (fig. S6B). We evaluated whether additional contacts could be established by replacing $Lys^2$ by an Arg residue (**C5**, Fig. 2). However, the binding affinity of **C5** measured by ITC was not improved (Table 1). We also explored the possibility to increase the binding affinity by varying $Leu^{U5}$ side chain. Four additional chimeras were synthetized with several alkyl and aryl side chains at position 5, $Nle^U$, $hPhe^U$, $Nal^U$, and $diF^U$ in the chimera **C6** to **C9**, respectively (Fig. 2). Although some were equally tolerated ($Nle^U$ in **C6** and $diF^U$ in **C9**), none of these modifications improved the binding affinity of **C2** (Table 1 and figs. S2 and S5). We lastly evaluated the consequence of extending the N terminus of **C2** with a capping box and synthesized **C10** terminated by the Ala-Ser-Thr-Glu tetrad (Fig. 2, Table 1, and figs. S2 and S5). In contrast to **P1**, this modification did not lead to a tighter binding. This result can, in part, be explained by the fact that the helix in ASF1-bound **C2** is tilted compared to the cognate α helix in **ip4**, so the extension of the helix may potentially induce a clash with ASF1-$Ala^{48}$ and $Glu^{49}$ residues.

### The chimera C2 is protected from proteolysis and penetrates in cells

We have previously shown that the oligourea backbone is far less susceptible to proteolysis than α-peptides and can be used as molecular insert to increase the stability of bioactive peptides (*11*, *19*). To evaluate whether α to urea replacement in the sequence of ASF1 ligands provide compounds with improved resistance to proteolytic degradation, we quantified the degradation rate of **C2** in human plasma and compared it to that of **P4** (Fig 5). The halftime of **P4** in human plasma was determined by following the decay of the intact molecule by liquid chromatography–mass spectrometry (LC-MS).

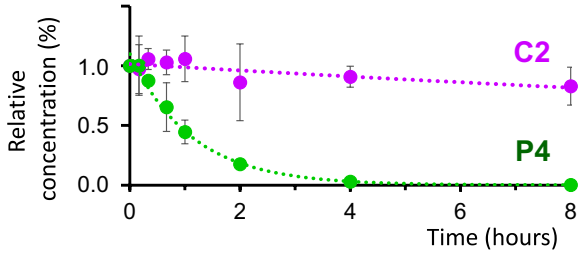


**Fig. 5. Stability against protease degradation in human plasma.** Stability against protease degradation in human plasma. The percentage of peptide **P4** or chimera **C2** detected by LC-MS is reported as a function of time. Error bars represent SD from three independent experiments.

In these conditions, **P4** had a lifetime of about 1 hour. In contrast, **C2** was largely resistant to protease degradation even after 8 hours in human plasma and that despite the presence of flanking α-amino acid residues at both termini of its sequence. We thus conclude that replacing about half of α-amino acid residues by ureido residues in **P4** is enough to protect the peptide hybrid against serum proteases. The ability of this compound to penetrate into cells was visualized by confocal microscopy using a fluorescein isothiocyanate (FITC)–tagged version of **C2** and compared to FITC-**P4** (fig. S7A). We observe green fluorescent dots inside cells for both compounds, showing effective cell penetration and their probable association with intracellular vesicles. Quantification of chimera/peptide accumulation in cells was measured using flow cytometry. FITC-**C2** penetrates cells significantly, even at low extracellular concentrations (below the micromolar), but its accumulation remains a factor of ~5 lower compared to FITC-**P4** (fig. S7, B and C).

## DISCUSSION

We have designed the first generation of ASF1 ligands with a central foldamer backbone by engineering peptide sequences derived from the C terminus of histone H3 and introducing oligourea inserts. We demonstrate that these sequence specific peptide-foldamer hybrids bind their biological target with $K_d$ in the low micromolar range. We also report a unique x-ray crystal structure of a complex between ASF1 and the most potent compound in the series. In good agreement with biomolecular NMR studies, this structure shows that the helical bound conformation and the binding mode of the cognate peptide domain is retained. Notably, the crystal structure also shows mutual plasticity of the two partners upon binding and the formation of a noncanonical bent helical structure resulting from a modification of the typical intramolecular three-center H-bond pattern of oligoureas by a protein side chain ($Tyr^{112}$). This alteration allows helix bending favorable for the four anchor residues to interact simultaneously. Here, the plasticity of the helical oligourea backbone can thus be seen as an advantage asset and allow the foldamer to shape itself to the protein surface. In another noteworthy example reported recently, flexible units were deliberately introduced in aromatic oligoamide foldamers to engineer helix destabilization and sense chirality at the protein surface (*36*). Despite this mutual adaptation of the chimera and the protein, the low enthalpic contribution to the binding free energy measured by microcalorimetry gives room for further optimization of the packing at the complex interface. We also demonstrate that inserting four ureido residues in the center of the helix was sufficient to considerably protect against proteolysis in particularly stringent conditions. This increased stability of foldamers in biological fluids bodes well for the development of ASF1 ligands with prolonged duration of action in vivo. Another interesting feature of chimera **C2** is its ability to penetrate into cells, although to a lesser extent compared to the peptide **P4**. This difference could be due to the different net charge of these compounds (+2 and +3 for **C2** and **P4**, respectively). The bioavailability of these compounds and their affinity for the target still need further optimization for effective inhibition of ASF1 in cells. The strategy reported previously for peptide **ip4** consisting in connecting a central binding element to a distant anchor point via a tailored spacer has recently been applied to foldamer-peptide hybrids (*37*) and is likely to apply to chimera **C2** to eventually conceive potent second-generation ASF1 ligands (*30*).

## MATERIALS AND METHODS

### Chemistry

Foldamer/peptide hybrids were synthesized on solid support using succinimidyl (2-azidoethyl)carbamate as activated monomers for the elongation of oligourea segments, as previously reported (figs. S8 to S11) (*19*, *32*, *33*). Full details on chemical synthesis and purification of peptides and foldamers **C1** to **C10** are given in the Supplementary Materials.

### Expression and purification of ASF1

Recombinant human ASF1 [hASF1A(1-156)] was purified as already described from expression in *Escherichia coli* of a $(His)_6$–glutathione *S*-transferase (GST)–TEV site–Asf1 fusion protein using the pETM30 plasmid (*38*). Briefly, soluble $(His)_6$-tagged GST fusion protein was purified on reduced glutathione agarose beads (Sigma-Aldrich). After cleavage with recombinant $(His)_6$-Tobacco Etch Virus Protease (TEV) protease at room temperature overnight, the $(His)_6$-GST tag and the protease were trapped in a nickel-charged nitrilotriacetic acid (NTA) chelate immobilized onto agarose column (Macherey Nagel). The flow-through fraction containing ASF1 protein was further purified by anion exchange chromatography using a Resource Q 6-ml column (GE Healthcare). ASF1 was then concentrated using an Amicon device (Millipore), and the buffer was replaced with a 50 mM tris-HCl (pH 7.5). Unlabled ASF1 used for ITC experiments was purified from pellets of bacteria grown in LB medium and uniformly labeled ASF1 from bacteria gown in M9 minimal media supplemented with $(^{15}NH_4)Cl$ (0.5 g/liter; Eurisotop) as the sole nitrogen source and or $^{13}C$ glucose (2 g/liter; Eurisotop).

### Isothermal titration calorimetry

All ITC experiments were performed in a VP-ITC titration calorimeter (Microcal/Malvern) at 20°C, in a 50 mM tris-HCl (pH 7.5) buffer. Protein and peptides concentrations were set to values of 10 and 200 μM, respectively. Protein and peptide samples were prepared in the same buffer and degassed (ThermoVac, Malvern). After equilibrating the cell at 298 K, the rotating syringe (310 rpm) injected at intervals of 280 s, 6 μl of aliquots of peptide solution into the ASF1 solution previously introduced in the sample cell, until saturation was observed. Raw ITC data were processed with the Origin 7.0 Software (OriginLab, Malvern) using the One-Set of Sites fitting model. All ITC experiments were performed at least in duplicate. One representative curve for each peptide/chimera is shown in fig. S2.

### NMR studies–$^{1}$H-$^{15}$N heteronuclear single-quantum coherence

The binding mode of the constrained peptides was assessed using NMR spectroscopy. NMR experiments were performed at 293 K or 298 K on Bruker Avance II 600 MHz spectrometer equipped with a proton-optimized triple resonance NMR 'inverse' cryoprobe (TCI), (Bruker). Purified uniformly labeled $^{15}N$ hASF1A(1-156) was concentrated to 40 μM and exchanged in NMR buffer [50 mM tris-HCl (pH 7.5), 0.1 mM EDTA, 0.1 mM dextran sulfate sodium (DSS), 0.1 mM $NaN_3$, protease inhibitor cocktail (at the concentration recommended by the provider, Roche), and 10% $D_2O$]. Proton chemical shifts (in parts per million) were referenced relative to internal DSS, and $^{15}N$ reference was set indirectly relative to DSS using frequency ratios (*39*). NMR data were processed using Topspin (Bruker) and analyzed using Sparky (T. D. Goddard and D. G. Kneller, University of California San Francisco). Amide assignment was taken from (*38*). The titration experiments were performed by adding increasing amounts of concentrated peptide or chimera to the ASF1 sample. At each ASF1:peptide ratio, a two dimensional $^{1}H$-$^{15}N$ SOFAST HMQC (heteronuclear multiple-quantum coherence) spectrum was recorded. Changes in chemical shift were measured for all resonances for all recorded spectra. Assignments were obtained by following progressive variations of chemical shifts upon titration or with a standard triple resonance method using a uniformly $^{15}N$-$^{13}C$–labeled ASF1 sample complexed with an excess of peptide or chimera. Chemical shift variation was calculated with the following formula $\sqrt{(\delta^{b}_{HN} - \delta^{f}_{HN})^2 + (0.17(\delta^{b}_{N} - \delta^{f}_{N}))^2}$, where δ represents measured chemical shift value. b or f refers to the bound or free form, respectively, HN or N to the amide proton or nitrogen, respectively. The factor 0.17 corresponds to the scaling factors used to normalize the magnitude of the proton and nitrogen chemical shift changes (in parts per million) (*40*). At saturation of the peptide or chimera, the maximal chemical shift variation was plotted as a function of the residue number for 138 residues of the 156 residues of hASF1A(1-156) (fig. S3). This corresponds to 96% of the expected values, considering the 12 prolines.

The exchange rate between bound and free forms was rapid upon addition of the chimeras **C1** to **C11** (Fig. 3A, lower middle for **C2**). The dissociation constant of the complex was fitted from the plot of the normalized chemical shift variation in function of total chimera concentration (as shown for two residues in Fig. 3A, bottom right) using the following equation: $\Delta\delta_N = \left[(c_A + c_C + K_d) - \sqrt{(c_A + c_C + K_d)^2 - 4 c_A c_C}\right]/2$, where $c_A$ represents the total concentration of ASF1, $c_C$ represents the total concentration of added chimera, and $K_d$ represents the dissociation constant. $\Delta\delta_N$ is the chemical shift variation normalized with the maximal chemical shift variation measured at saturating concentration of chimera. For each chimera, the fit was performed independently ASF1 residues belonging to the three main regions showing significant chemical shift changes: $Ala^{48}$, $Glu^{49}$, $Glu^{51}$, $Val^{90}$, $Thr^{93}$, $Ile^{97}$, $Arg^{108}$, $Val^{109}$, and $Tyr^{111}$. These residues were chosen because (i) they show significant chemical shift variation (more than 0.07 ppm) and (ii) the signals allowed a precise measure of the chemical shift at all chimera concentrations (no suppositions and no slow-intermediate exchange rate). The value of the dissociation constant reported in Table 1 corresponds to the mean $K_d$ value and standard deviation (SD) fitted for these residues. Curves and fits are shown in fig. S4.

### Crystallization, data collection, and structure determination

hASF1A(1-156) and **C2** were mixed, and the complex was concentrated to 8.6 mg/ml in a buffer 50 mM tris-HCl (pH 7.4). Crystals of the complex were grown by sitting drop vapor diffusion at 20°C against reservoir solution containing 100 mM sodium citrate (pH 4.2), 300 mM $LiSO_4$, and 26% PEG3350 [Poly(ethylene glycol) Average Molecular Mass 3350]. Crystals were soaked in a 100 mM sodium citrate (pH 4.2), 300 mM $LiSO_4$, 26% PEG3350, and 20% glycerol cryo-protectant solution before being flash-frozen in liquid nitrogen. Diffraction data were collected on the PROXIMA-1 beamline at the Synchrotron SOLEIL (Saint Aubin, France) at a temperature of 100°K with an x-ray wavelength of 0.97857 Å. Diffraction images recorded with PILATUS 6M detector were processed using the XDS package (*41*). Best datasets were obtained from two crystals of hASF1A(1-156)–**C2** belonging to space group **P1**, which diffracted up to 1.8-Å resolution. The two datasets were merged and scaled, and the structure of ASF1A(1-156)–**C2** complex was determined by

molecular replacement using MOLREP (*42*) with the human ASF1A structure [chain A of Protein Data Bank (PDB) entry 2i32] as the model probe. Best solution contained two complexes per asymmetric unit. Model building was performed with the Coot software (*43*), and structure refinement was achieved with BUSTER version 2.10 (*44*, *45*). Final refinement statistics are presented in table S2. Structure representations presented in all figures were drawn with PyMOL software (Schrödinger).

### Proteolysis assay

Stock solutions of the peptide **P4** and the chimera **C2** were prepared at a concentration of 250 μM in water. Stock solution of human plasma was prepared in water as aliquots. Each aliquot was diluted 1/4 with a solution of 0.1 M phosphate-buffered saline (PBS) (pH7.4) buffer before use. Stability of these molecules in human plasma was assessed by conducting protease reaction at 37°C. A total of 392 μl of the solution of human plasma in PBS was first incubated for 15 min at 37°C. To this, preactivated enzymatic solution was added 8 μl of the solution of the tested compound (final concentration, 5 μM). At the indicated times (0, 10, 20, 40, 60, 120, 240, and 480 min), an aliquot of 45 μl was collected and added to 150 μl of acetonitrile (ACN) to quench the reaction. The samples were frozen at −80°C before analysis. The frozen samples were defrosted, stirred with a vortex (2 min), and lastly centrifuged (16°C, 5 min, 18,000*g*). A portion of the resulting supernatant was submitted to concentration under high vacuum to remove ACN excess and then resuspended in a solution of water +0.1% formic acid/ACN + 0.1% formic acid (95:5, v/v). Reaction progress over time was quantified by UPLC-MS analysis. The time course of inhibitor degradation was determined by integrating the area of the peak from the extracted ion chromatogram. All experiments were carried out in triplicates for both compounds. The chromatography conditions were as following: Column: Phenomenex Aeris PEPTIDE 1.7 μm XB-C18: 150 mm × 2.1 mm; mobile phase: A = water with 0.1% formic acid, B = acetonitrile with 0.1% formic acid; gradient: A/B (95:5) for 1.0 min to A/B (60:40) over 5 min to A/B (90:10) for 1.5 min to A/B (95:5) for 2.5 min; flow rate: 0.5 ml/min; temperature: 60°C; instrument: Dionex Ultimate 3000 (Thermo Fisher Scientific); detection: electrospray ionization–FTMS (Fourier Transform Mass Spectrometry) in positive mode (150 to 2000 mass/charge ratio) on a Q Exactive instrument (Thermo Fisher Scientific).

### Cell penetration assays

Human cancer cell lines U2OS [osteosarcoma (ATCC HTB-96)] were cultured in Dulbecco's modified Eagle medium (Sigma-Aldrich) containing 10% (v/v) fetal bovine serum (FBS; Sigma-Aldrich) and penicillin (100 U/ml) and streptomycin (100 μg/ml) (Gibco) at 37°C in a humidified incubator with 5% $CO_2$. For quantification of peptide/chimera penetration by fluorescence-activated cell sorting, U2OS cells were seeded in 24-well plates at 50,000 cells per well and incubated for 48 hours at 37°C and 5% $CO_2$. Then, FITC peptide/chimera was added directly into the culture medium (v/v) at final concentrations of 0.5, 1, 3, 5, or 10 μM, and cells were incubated 24 hours at 37°C and 5% $CO_2$. The culture medium was removed, and cells were rinsed twice with PBS (Sigma-Aldrich, D8537). Cells were then incubated with trypsin (5 mg/ml)–EDTA (2 mg/ml) (Sigma-Aldrich, T4174) at 37°C and 5% $CO_2$, with dual purpose of detaching the cells and removing most of the peptides/chimera nonspecifically adhering to the extracellular membrane (*46*). Cells were transferred to 1.5-ml tubes and washed twice with PBS buffer complemented with 2% FBS and 2 mM EDTA. Propidium ionide (PI) was added at 1 μg/ml final concentration to probe dead/dying cells. Flow cytometry analysis was then immediately performed using a Guava easyCyte HT instrument (Millipore) with a total of 10,000 events recorded per sample. The FITC fluorescence intensity of peptide/chimera was measured for intact cells in the green channel ($\lambda_{Ex}$ 488 nm and $\lambda_{Em}$ 525/30 nm). The percentage of damaged cells was measured in the red channel with PI fluorescence ($\lambda_{Ex}$ 488 nm and $\lambda_{Em}$ 680/30 nm). It was less than 10% for all samples.

For visualization of peptide/chimera penetration by microscopy, U2OS cells were seeded into the wells of a collagen-coated (Sigma-Aldrich) optical 96-well culture plate (Ibidi) at a final density of 1500 cells per well. Plates were then incubated for 48 hours at 37°C and 5% $CO_2$ to allow cell adhesion. The supernatant was removed and replaced with fresh medium containing either FITC-P2, FITC-P4, or $H_2O$ (vehicle) as control, and plates were incubated for 24 additional hours at 37°C and 5% $CO_2$. Cells were then fixed with paraformaldehyde [4% (w/v) final], and nuclear DNA was fluorescently labeled by Hoechst 33342 (2 μg/ml final). After an overnight incubation at 4°C, supernatants were removed by aspiration and replaced by 100 μl of PBS. Plates were imaged on a confocal microscope (Nikon Ti2 equipped with a spinning disk module) in the blue (Hoechst) channel ($\lambda_{Ex}$ 405 nm and $\lambda_{Em}$ 460/50 nm) and in the green (FITC) channel ($\lambda_{Ex}$ 488 nm and $\lambda_{Em}$ 535/50 nm) at ×20 magnification. Images were imported in Fiji (*47*), and image and contrast were adjusted using the image (FITC-**C2** at 10 μM) as reference for comparison purposes.

## SUPPLEMENTARY MATERIALS

Supplementary material for this article is available at http://advances.sciencemag.org/cgi/content/full/7/12/eabd9153/DC1

View/request a protocol for this paper from *Bio-protocol*.

## REFERENCES AND NOTES


1. M. Pasco, G. Dolain, G. Guichard, in *Comprehensive Supramolecular Chemistry II*, J. L. Atwood, G. W. Gokel, L. J. Barbour, Eds. (Elsevier, 2017), vol. 5, chap. 5.05, pp. 89–125.
2. R. Gopalakrishnan, A. I. Frolov, L. Knerr, W. J. Drury III, E. Valeur, Therapeutic potential of foldamers: From chemical biology tools to drug candidates? *J. Med. Chem.* **59**, 9599–9621 (2016).
3. E. Valeur, S. M. Guéret, H. Adihou, R. Gopalakrishnan, M. Lemurell, H. Waldmann, T. N. Grossmann, A. T. Plowright, New modalities for challenging targets in drug discovery. *Angew. Chem. Int. Ed. Eng.* **56**, 10294–10323 (2017).
4. V. Azzarito, K. Long, N. S. Murphy, A. J. Wilson, Inhibition of α-helix-mediated protein-protein interactions using designed molecules. *Nat. Chem.* **5**, 161–173 (2013).
5. W. S. Horne, T. N. Grossmann, Proteomimetics as protein-inspired scaffolds with defined tertiary folding patterns. *Nat. Chem.* **12**, 331–337 (2020).
6. R. J. Simon, R. S. Kania, R. N. Zuckermann, V. D. Huebner, D. A. Jewell, S. Banville, S. Ng, L. Wang, S. Rosenberg, C. K. Marlowe, Peptoids: A modular approach to drug discovery. *Proc. Natl. Acad. Sci. U.S.A.* **89**, 9367–9371 (1992).
7. J. Frackenpohl, P. I. Arvidsson, J. V. Schreiber, D. Seebach, The outstanding biological stability of beta- and gamma-peptides toward proteolytic enzymes: An in vitro investigation with fifteen peptidases. *Chembiochem* **2**, 445–455 (2001).
8. D. Seebach, A. K. Beck, D. J. Bierbaum, The world ofβ- andγ-peptides comprised of homologated proteinogenic amino acids and other components. *Chem. Biodivers.* **1**, 1111–1239 (2004).
9. C. M. Grison, J. A. Miles, S. Robin, A. J. Wilson, D. J. Aitken, An α-helix-mimicking 12,13-helix: Designed α/β/γ-foldamers as selective inhibitors of protein-protein interactions. *Angew. Chem. Int. Ed. Eng.* **55**, 11096–11100 (2016).
10. P. Sang, M. Zhang, Y. Shi, C. Li, S. Abdulkadir, Q. Li, H. Ji, J. Cai, Inhibition of β-catenin/B cell lymphoma 9 protein-protein interaction using α-helix–mimicking sulfono-γ-AA peptide inhibitors. *Proc. Natl. Acad. Sci. U.S.A.* **116**, 10757–10762 (2019).
11. E. Teyssières, J.-P. Corre, S. Antunes, C. Rougeot, C. Dugave, G. Jouvion, P. Claudon, G. Mikaty, C. Douat, P. L. Goossens, G. Guichard, Proteolytically stable foldamer mimics

of host-defense peptides with protective activities in a murine model of bacterial infection. *J. Med. Chem.* **59**, 8221–8232 (2016).
12. S. Liu, R. W. Cheloha, T. Watanabe, T. J. Gardella, S. H. Gellman, Receptor selectivity from minimal backbone modification of a polypeptide agonist. *Proc. Natl. Acad. Sci. U.S.A.* **115**, 12383–12388 (2018).
13. M. V. Hager, L. M. Johnson, D. Wootten, P. M. Sexton, S. H. Gellman, β-Arrestin-biased agonists of the GLP-1 receptor from beta-amino acid residue incorporation into GLP-1 analogues. *J. Am. Chem. Soc.* **138**, 14970–14979 (2016).
14. K. J. Peterson-Kaufman, H. S. Haase, M. D. Boersma, E. F. Lee, W. D. Fairlie, S. H. Gellman, Residue-based preorganization of BH3-derived α/β-Peptides: Modulating affinity, aelectivity and proteolytic susceptibility in α-helix mimics, selectivity and proteolytic susceptibility in α-helix mimics. *ACS Chem. Biol.* **10**, 1667–1675 (2015).
15. S. Kumar, M. Birol, D. E. Schlamadinger, S. P. Wojcik, E. Rhoades, A. D. Miranker, Foldamer-mediated manipulation of a pre-amyloid toxin. *Nat. Commun.* **7**, 11412 (2016).
16. L. M. Johnson, S. H. Gellman, α-Helix mimicry with alpha/beta-peptides. *Methods Enzymol.* **523**, 407–429 (2013).
17. W. S. Horne, L. M. Johnson, T. J. Ketas, P. J. Klasse, M. Lu, J. P. Moore, S. H. Gellman, Structural and biological mimicry of protein surface recognition by alpha/beta-peptide foldamers. *Proc. Natl. Acad. Sci. U.S.A.* **106**, 14751–14756 (2009).
18. R. W. Cheloha, A. Maeda, T. Dean, T. J. Gardella, S. H. Gellman, Backbone modification of a polypeptide drug alters duration of action in vivo. *Nat. Biotechnol.* **32**, 653–655 (2014).
19. J. Fremaux, C. Venin, L. Mauran, R. H. Zimmer, G. Guichard, S. R. Goudreau, Peptide-oligourea hybrids analogue of GLP-1 with improved action in vivo. *Nat. Commun.* **10**, 924 (2019).
20. C. M. Lombardo, V. Kumar M. V., C. Douat, F. Rosu, J. L. Mergny, G. F. Salgado, G. Guichard, Design and structure determination of a composite zinc finger containing a nonpeptide foldamer Helical domain. *J. Am. Chem. Soc.* **141**, 2516–2525 (2019).
21. J. Fremaux, L. Mauran, K. Pulka-Ziach, B. Kauffmann, B. Odaert, G. Guichard, α-Peptide-oligourea chimeras: Stabilization of short alpha-helices by non-peptide helical foldamers. *Angew. Chem. Int. Ed. Eng.* **54**, 9816–9820 (2015).
22. R. J. Burgess, Z. Zhang, Histone chaperones in nucleosome assembly and human disease. *Nat. Struct. Mol. Biol.* **20**, 14–22 (2013).
23. F. Abascal, A. Corpet, Z. A. Gurard-Levin, D. Juan, F. Ochsenbein, D. Rico, A. Valencia, G. Almouzni, Subfunctionalization via adaptive evolution influenced by genomic context: The case of histone chaperones ASF1a and ASF1b. *Mol. Biol. Evol.* **30**, 1853–1866 (2013).
24. J. S. Im, M. Keaton, K. Y. Lee, P. Kumar, J. Park, A. Dutta, ATR checkpoint kinase and CRL1 TRCP collaborate to degrade ASF1a and thus repress genes overlapping with clusters of stalled replication forks. *Genes Dev.* **28**, 875–887 (2014).
25. A. Corpet, L. de Koning, J. Toedling, A. Savignoni, F. Berger, C. Lemaître, R. J. O'Sullivan, J. Karlseder, E. Barillot, B. Asselain, X. Sastre-Garau, G. Almouzni, Asf1b, the necessary Asf1 isoform for proliferation, is predictive of outcome in breast cancer. *EMBO J.* **30**, 480–493 (2011).
26. X. Liang, X. Yuan, J. Yu, Y. Wu, K. Li, C. Sun, S. Li, L. Shen, F. Kong, J. Jia, M. Björkholm, D. Xu, Histone chaperone ASF1A predicts poor outcomes for patients with gastrointestinal cancer and Drives cancer progression by stimulating transcription of β-catenin target genes. *EBioMedicine* **21**, 104–116 (2017).
27. Y. Wu, X. Li, J. Yu, M. Bjorkholm, D. Xu, ASF1a inhibition induces p53-dependent growth arrest and senescence of cancer cells. *Cell Death Dis.* **10**, 76 (2019).
28. F. Mousson, A. Lautrette, J. Y. Thuret, M. Agez, R. Courbeyrette, B. Amigues, E. Becker, J. M. Neumann, R. Guerois, C. Mann, F. Ochsenbein, Structural basis for the interaction of Asf1 with histone H3 and its functional implications. *Proc. Natl. Acad. Sci. U.S.A.* **102**, 5975–5980 (2005).
29. C. M. English, M. W. Adkins, J. J. Carson, M. E. Churchill, J. K. Tyler, Structural basis for the histone chaperone activity of Asf1. *Cell* **127**, 495–508 (2006).
30. M. Bakail, A. Gaubert, J. Andreani, G. Moal, G. Pinna, E. Boyarchuk, M. C. Gaillard, R. Courbeyrette, C. Mann, J. Y. Thuret, B. Guichard, B. Murciano, N. Richet, A. Poitou, C. Frederic, M. H. le du, M. Agez, C. Roelants, Z. A. Gurard-Levin, G. Almouzni, N. Cherradi, R. Guerois, F. Ochsenbein, Design on a rational basis of high-affinity peptides inhibiting the histone chaperone ASF1. *Cell Chem. Biol.* **26**, 1573–1585.e10 (2019).
31. R. Aurora, G. D. Rose, Helix capping. *Protein Sci.* **7**, 21–38 (1998).
32. G. W. Collie, K. Pulka-Ziach, C. M. Lombardo, J. Fremaux, F. Rosu, M. Decossas, L. Mauran, O. Lambert, V. Gabelica, C. D. Mackereth, G. Guichard, Shaping quaternary assemblies of water-soluble non-peptide helical foldamers by sequence manipulation. *Nat. Chem.* **7**, 871–878 (2015).
33. C. Douat-Casassus, K. Pulka, P. Claudon, G. Guichard, Microwave-enhanced solid-phase synthesis of N,N'-linked aliphatic oligoureas and related hybrids,N'-linked aliphatic oligoureas and related hybrids. *Org. Lett.* **14**, 3130–3133 (2012).
34. Y. Tang, M. V. Poustovoitov, K. Zhao, M. Garfinkel, A. Canutescu, R. Dunbrack, P. D. Adams, R. Marmorstein, Structure of a human ASF1a-HIRA complex and insights into specificity of histone chaperone complex assembly. *Nat. Struct. Mol. Biol.* **13**, 921–929 (2006).
35. L. Fischer, P. Claudon, N. Pendem, E. Miclet, C. Didierjean, E. Ennifar, G. Guichard, The canonical helix of urea oligomers at atomic resolution: Insights into folding-induced axial organization. *Angew. Chem. Int. Ed. Eng.* **49**, 1067–1070 (2010).
36. M. Vallade, P. Sai Reddy, L. Fischer, I. Huc, Enhancing aromatic foldamer helix dynamics to probe interactions with protein surfaces. *Eur. J. Org. Chem.* **2018**, 5489–5498 (2018).
37. G. M. Burslem, H. F. Kyle, A. L. Breeze, T. A. Edwards, A. Nelson, S. L. Warriner, A. J. Wilson, Towards "bionic" proteins: Replacement of continuous sequences from HIF-1α with proteomimetics to create functional p300 binding HIF-1α mimics. *Chem. Commun. (Camb.)* **52**, 5421–5424 (2016).
38. F. Mousson, J. Couprie, J. Y. Thuret, J. M. Neumann, C. Mann, F. Ochsenbein, 1H, 13C and 15N resonance assignments of the conserved core of hAsf1 A. *J. Biomol. NMR* **29**, 413–414 (2004).
39. D. S. Wishart, C. G. Bigam, J. Yao, F. Abildgaard, H. J. Dyson, E. Oldfield, J. L. Markley, B. D. Sykes, 1H, 13C and 15N chemical shift referencing in biomolecular NMR. *J. Biomol. NMR* **6**, 135–140 (1995).
40. B. T. Farmer II, K. L. Constantine, V. Goldfarb, M. S. Friedrichs, M. Wittekind, J. Yanchunas Jr., J. G. Robertson, L. Mueller, Localizing the NADP+ binding site on the MurB enzyme by NMR. *Nat. Struct. Biol.* **3**, 995–997 (1996).
41. W. Kabsch, Integration, scaling, space-group assignment and post-refinement. *Acta Crystallogr. D Biol. Crystallogr.* **66**, 133–144 (2010).
42. A. Vagin, A. Teplyakov, Molecular replacement withMOLREP. *Acta Crystallogr. D Biol. Crystallogr.* **66**, 22–25 (2010).
43. P. Emsley, K. Cowtan, Coot: Model-building tools for molecular graphics. *Acta Crystallogr. D Biol. Crystallogr.* **60**, 2126–2132 (2004).
44. G. Bricogne et al., BUSTER version 2.10. *Cambridge, United Kingdom: Global Phasing Ltd.*, (2017).
45. O. S. Smart, T. O. Womack, C. Flensburg, P. Keller, W. Paciorek, A. Sharff, C. Vonrhein, G. Bricogne, Exploiting structure similarity in refinement: Automated NCS and target-structure restraints in BUSTER. *Acta Crystallogr. D Biol. Crystallogr.* **68**, 368–380 (2012).
46. Q. Seisel, F. Pelletier, S. Deshayes, P. Boisguerin, How to evaluate the cellular uptake of CPPs with fluorescence techniques: Dissecting methodological pitfalls associated to tryptophan-rich peptides. *Biochim. Biophys. Acta Biomembr.* **1861**, 1533–1545 (2019).
47. J. Schindelin, I. Arganda-Carreras, E. Frise, V. Kaynig, M. Longair, T. Pietzsch, S. Preibisch, C. Rueden, S. Saalfeld, B. Schmid, J. Y. Tinevez, D. J. White, V. Hartenstein, K. Eliceiri, P. Tomancak, A. Cardona, Fiji: An open-source platform for biological-image analysis. *Nat. Methods* **9**, 676–682 (2012).
48. E. D. Goddard-Borger, R. V. Stick, An efficient, inexpensive, and shelf-stable diazotransfer reagent: Imidazole-1-sulfonyl azide hydrochloride. *Org. Lett.* **9**, 3797–3800 (2007).

**Acknowledgments:** We thank the Synchrotron SOLEIL, the European Synchrotron Radiation Facility (ESRF), and the French Infrastructure for Integrated Structural Biology (FRISBI) ANR-10-INBS-05. We are particularly grateful to A. Clavier and A. Campalans for help in setting up and performing the cell penetration assays. **Funding:** Research was funded by the French Centre National de Recherche Scientifique (CNRS), the Commissariat à l'Energie Atomique (CEA), University of Bordeaux, University Paris-Saclay, and the Synchrotron Soleil. The project was supported by the ANR 2007 BREAKABOUND (JC-07-216078), 2011 BIPBIP (ANR-10-BINF-0003), 2012 CHAPINHIB (ANR-12-BSV5-0022-01), 2015 CHIPSET (ANR-15-CE11-008-01), 2015 CHIMPP2I (ANR-15-CE07-0010), and the program labeled by the ARC foundation 2016 (PGA1*20160203953). M.B. was supported by Canceropole (Paris, France) and a grant for young researchers from La Ligue contre le Cancer. J.M. was supported by La Ligue contre le Cancer. **Author contributions:** C.D., R.G., G.G., and F.O. designed ASF-1 foldamer ligands. J.M., C.A., and M.E.P. synthesized the ligands and analyzed results. M.B., M.E.P., P.L., S.T., and F. O. performed biochemical, biophysical studies and structural studies and analyzed results. M.E.P., F.B., G.M., G.P., and F.O. performed the human plasma degradation assay cell penetration studies and analyzed results. R.G., G.G., and F.O. conceived the project. F.O. supervised the project. G.G. and F.O. analyzed the data. The manuscript was written through contributions of all authors. **Competing interests:** The authors declare that they no competing interests. **Data and materials availability:** All data needed to evaluate the conclusions in the paper are present in the paper and/or the Supplementary Materials. The accession number of the structure in the PDB is 6ZUF. Additional data related to this paper may be requested from the authors.

Submitted 23 July 2020
Accepted 27 January 2021
Published 19 March 2021
10.1126/sciadv.abd9153

**Citation:** J. Mbianda, M. Bakail, C. André, G. Moal, M. E. Perrin, G. Pinna, R. Guerois, F. Becher, P. Legrand, S. Traoré, C. Douat, G. Guichard, F. Ochsenbein, Optimal anchoring of a foldamer inhibitor of ASF1 histone chaperone through backbone plasticity. *Sci. Adv.* **7**, eabd9153 (2021).

Science Advances

# Optimal anchoring of a foldamer inhibitor of ASF1 histone chaperone through backbone plasticity

Johanne Mbianda, May Bakail, Christophe André, Gwenaëlle Moal, Marie E. Perrin, Guillaume Pinna, Raphaël Guerois, Francois Becher, Pierre Legrand, Seydou Traoré, Céline Douat, Gilles Guichard and Françoise Ochsenbein

*Sci Adv* **7** (12), eabd9153.
DOI: 10.1126/sciadv.abd9153